Ceramics-Silikáty 66 (3), 339-346 (2021)
www.ceramics-silikaty.cz doi: 10.13168/cs.2022.0029

MECHANICAL PROPERTIES AND MICROSTRUCTURE OF SALINE SOIL SOLIDIFIED BY ALKALI-ACTIVATED STEEL SLAG

WANG JIANING*, #HUANG LEI*,**, WU CHENGYOU*,**, JIANG TAO***,****

*Department of Civil Engineering, Qinghai University, Xining 810016, China
**Qinghai Provincial Key Laboratory of Energy-saving Building Materials and Engineering Safety, Xining 810016, China
***Qinghai Building and Materials Research Co., Ltd, Xining 810016, China
****Qinghai Provincial Key Laboratory of Plateau Green Building and Eco-community, Xining 810016, China

#E-mail: leihyx@foxmail.com

Submitted April 15, 2022; accepted May 30, 2022

Keywords: Solidified soil, Alkali activation, Unconfined compressive strength, Ultrasonic, Gelatinous products

The work aims to investigate the possibility of modifying and improving the mechanical properties of saline soil by incorporating alkali-activated steel slag (A-SS). The unconfined compressive strength of the solidified soil and the propagation velocity of the ultrasound in the solidified soil were tested. Moreover, the morphology of the microstructure was observed, and the chemical composition of the solidified soil was analysed. The results show that A-SS incorporation can improve the mechanical properties of saline soil, especially when the dosage of A-SS incorporation exceeds 15 %, the unconfined compressive strength of the soil can be significantly increased. The ultrasonic tests show that the ultrasound propagates faster in the solidified soil than in the original soil. The microstructure of the solidified soil with A-SS incorporation is much more compact than the original soil. Soil particles are combined by the formed gelatinous products, C-A-S-H and C-A-H, existing in a continuous form, which accounts for the noticeable increase in the unconfined compressive strength and the faster propagation velocity of the ultrasound in the specimens. Therefore, the solidification of saline soil by alkali-activated steel slag is feasible.

INTRODUCTION

Saline soil refers to a soil whose salt content exceeds a certain amount. It is widely distributed in China, but mainly distributed in western China. The total area of saline soil in the region accounts for more than 66 % of the total area of saline soil in China [1]. Based on its composition, saline soil could be classified as sulfate saline soil or chloride saline soil. Compared to general soil, the existence of a high salt soil leads to the characteristics of corrosiveness, dissolution, and salt swelling [2, 3], which often cause or aggravate problems in construction engineering and road engineering, such as corrosion, salt heaving, churning, frost heaving and other engineering issues. Thus, numerous techniques have been adopted to eliminate or avoid the above engineering problems in road sections and areas with a salt content exceeding the design standard. The measures include soil replacement, strong tamping, vibration compaction, aggregate solidification, and chemical stabilisation [4–6].

As the most widely used construction building materials, ordinary Portland cement (OPC) is thought to be the first choice to stabilise the soil. Some researchers mixed OPC with in situ soil at the intended depth and found that the mechanical properties of the problematic soil could be effectively improved by OPC [7, 8]. However, it is well known that the manufacturing process of OPC leads to high energy consumption and carbon emissions [9], and these two factors cause huge environmental problems [10]. The partial replacement of OPC by pozzolanic materials was a choice to overcome the above-stated problems. Pourakbar et al. [11] investigated the possible uses of palm oil fuel ash (individually and in combination with OPC) on the basic properties of clayey soils, the results showed that the treatments led to a significant reduction in the soil plasticity index and the optimum moisture content, but only when the palm oil fuel ash combined with cement the unconfined compressive strength could be significantly increased. Al-Amoudi [12] used cement and lime at different dosages to stabilise sabkha soil, the author found that

only the cement succeeded in improving the strength of the soil, the maximum unconfined compressive strength was attained at lower moisture contents than the optimum. Chai [13] reported that using conventional building materials, such as lime and fly ash with a small quantity of liquid polymer materials to modify and solidify the coastal saline soil could significantly improve the strength and water stability of the soil. Besides, it also has the advantages of simple construction and low cost. Some other researchers conducted similar studies and found that the replacement of OPC by pozzolanic materials was limited to low amounts [14,15].

Steel slag is a waste slag discharged in the process of steelmaking. With the improvement of environmental awareness, the rational utilisation of steel slag has attracted more and more attention. Zhang et al. [16] used a higher NaOH content and a lower water binder ratio to prepare an alkali-activated steel slag (A-SS) slurry, and found that its compressive strength at 28 d was 26 MPa. The C-S-H gel and the crystalline $Si_2Al_2O_5(OH)_4$ were found as the main hydration products. Also, the author added silica fume and graphene to improve the performance of the slurry [17]. As a result, the hydration products were C-S-H gel and pyrophyllite. Wang et al. [18] studied the effect of different contents of NaOH on the hydration properties of A-SS. The results showed that an increase in the initial alkalinity can promote the early hydration of the active components of the steel slag, but has little effect on the later hydration degree. The hydration products are still C-S-H gel and $Ca(OH)_2$. Compared with cement, the amount of hydration products of a steel slag activated by NaOH is much less than that in cement. Liu et al. [19] used sodium silicate to activate steel slag and studied the early hydration reactions of A-SS under high-temperature curing conditions. The results showed that the hydration products were $Ca(OH)_2$, N-A-S-H gel, and C-A-S-H gel.

The application of A-SS as construction building materials meets the current engineering needs and its effective use as solid waste. The work explored the possibility of utilising A-SS as a stabiliser for saline soil. In addition, the mechanical performance of the solidified soil was investigated. Meanwhile, the microstructure and the chemical compositions of the solidified soil were investigated.

EXPERIMENTAL

Raw materials

The raw soil used in the study was obtained from Haidong City, Qinghai Province. The chemical compositions of the saline soil and steel slag are shown in Table 1, the X-ray diffraction (XRD) patterns of the saline soil and the steel slag are shown in Figure 1. The optimum moisture content of the saline soil is 20.3 % and the actual moisture content is 10.1 %. Sodium silicate solution, with a mass fraction of 66.49 % and a module of 3.3, was used as the stock solution of the alkali activator.

Sample Preparation

The module of the alkali activator was set as 2 in the study. The mix proportion of the A-SS is shown in Table 2, the water to binder ratio of A-SS was kept at 20.3 %, based on the optimum moisture content of the saline soil.

Table 1. Chemical composition of the saline soil and steel slag (%).

Composition	SiO_2	SO_3	CaO	Fe_2O_3	Al_2O_3	K_2O	Na_2O	TiO_2	MgO	Cl
Saline soil	32.4	24.6	15.9	9.69	9.42	2.85	1.94	1.26	0.47	0.32
Steel slag	20.1	1.16	41.8	16.3	8.78	0.52	0.43	0	11.1	0

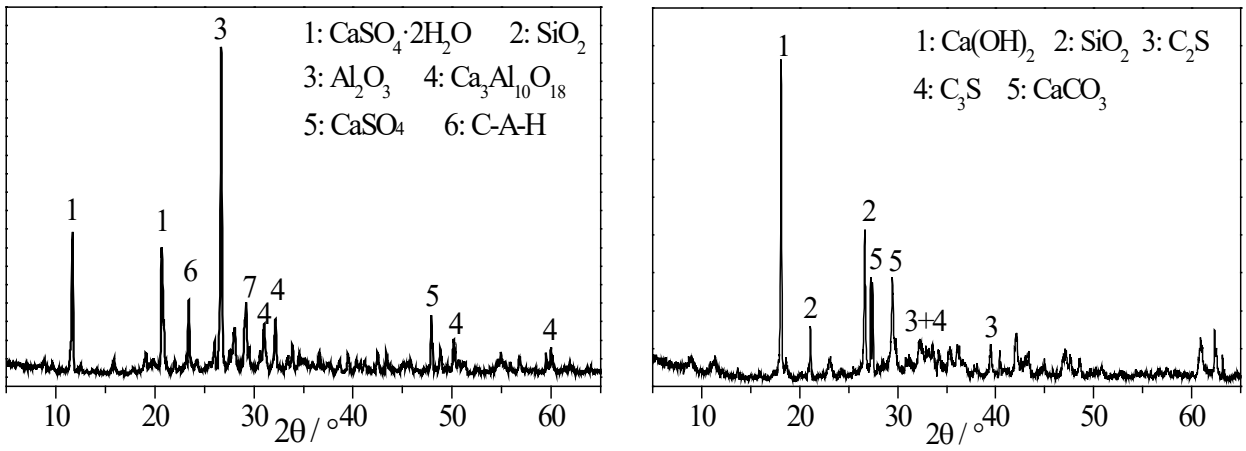

Figure 1. XRD patterns of the saline soil and steel slag.

Table 2. Mix proportion of the A-SS (wt. %).

Steel slag	Sodium silicate (L)	NaOH (S)	Water
71.30	23.60	3.38	1.73

The soil was dried in the air and the soil agglomerates were ground. Then the ground soil was screened through a 2 mm square hole sieve. Saline soil particles measuring less than 2 mm were used for the test. The mix proportions of the solidified soil are shown in Table 3, the mass fractions of the A-SS of the solidified soil were set as 10 %, 12 %, and 15 %. The total moisture content of the soil was kept at 20.3 %.

Table 3. Mix proportions of the solidified soil (wt. %).

Specimens	A-SS	Saline soil	Water
S	0	91.52	8.48
SAS10	10	82.37	7.63
SAS12	12	80.54	7.46
SAS15	15	77.79	7.21

According to the proportion shown in Table 2, the steel slag and alkali activator were mixed, and slow stirring for 60 s was conducted by a cement paste mixer (JJ-5). Then, the screened saline soil and water, based on the mix proportions shown in Table 3, were added to the mixer. One proceeded successively by slow stirring for 60 s, followed by a pause of 30 s, and then rapid stirring for 60 s. After that, the mixing pot was covered with a fresh-keeping film. Meanwhile, a certain amount of the specimen was taken out and moulded with a portable compactor. Finally, the moulded samples were covered with a fresh-keeping film and cured in a room at 20 °C with 95 % relative humidity (RH).

Test method

A microcomputer-controlled electronic universal testing machine was used to test the unconfined compressive strength of the specimens at 7 d and 28 d. A non-metallic ultrasonic testing analyser (NM-4B, Koncrete, Beijing, China) was applied to test the propagation velocity of the ultrasound in the specimens at 3 d, 7 d, and 28 d to explore the inner characteristics of the specimens.

After the mechanical test, the crushed specimens were collected for a microscopic analysis. The crushed specimens were dried in an oven at 80 °C for 6 h. Then, a piece of the dried specimen was sprayed with gold and prepared to observe the microstructure, by using a scanning electron microscope (SEM, JSM-6610LV, JEOL, Ltd., Tokyo, Japan).

Another part of the dried specimen was ground in an agate mortar until there was no obvious graininess in the powder of the specimens. The X-ray diffraction (XRD) patterns of the specimens were collected by an X-ray diffractometer (D/max-2500PC, Rigaku Corporation, Tokyo, Japan) with an acceleration voltage of 30 kV, the 2θ was in the range of 5 to 65° and the scanning speed was kept as 6°·min^{-1}.

RESULTS AND DISCUSSION

Mechanical Properties

Figure 2 shows the unconfined compressive strength of the solidified soil at 7 d and 28 d. The unconfined compressive strength of SAS10, SAS12, and SAS15 increased by 0.93 %, 21.32 %, and 170.37 %, respectively, compared to that of S at 7 d. It could be inferred that there is a key value of the incorporation quantity of A-SS for the unconfined compressive strength of the solidified soil, which is between 12 % and 15 %. When the incorporation quantity of A-SS exceeds the key value, the unconfined compressive strength of the solidified soil would be significantly improved. With the prolongation of the curing age, the unconfined compressive strength of the solidified soil develops differently. The unconfined compressive strength of S is weakened by 41.67 % at 28 d compared to that at 7 d, whereas for the solidified soil, the unconfined compressive strength is strengthened with an increase in the age, especially for the specimen with a high dosage of A-SS incorporation.

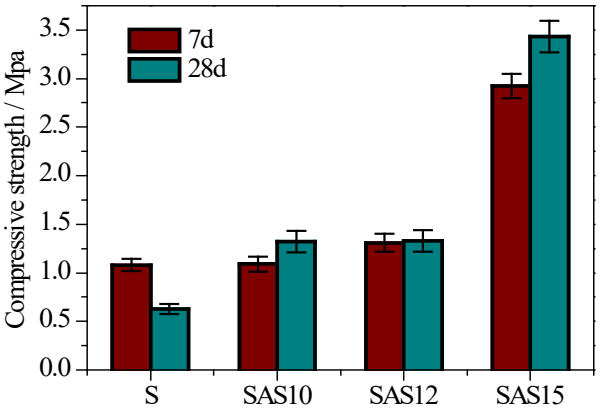

Figure 2. Unconfined compressive strength.

It is known that the hydration activity of steel slag in water is poor, it would take a period of time for the reaction of the steel slag [20]. The difference in the variation trend of the unconfined compressive strength for the original soil and the solidified soil could be due to the slow reaction of the steel slag. For S, the original saline soil, the mechanical property is weakened due to some specific variations which need to be further studied. For the solidified soil, in addition to the specific

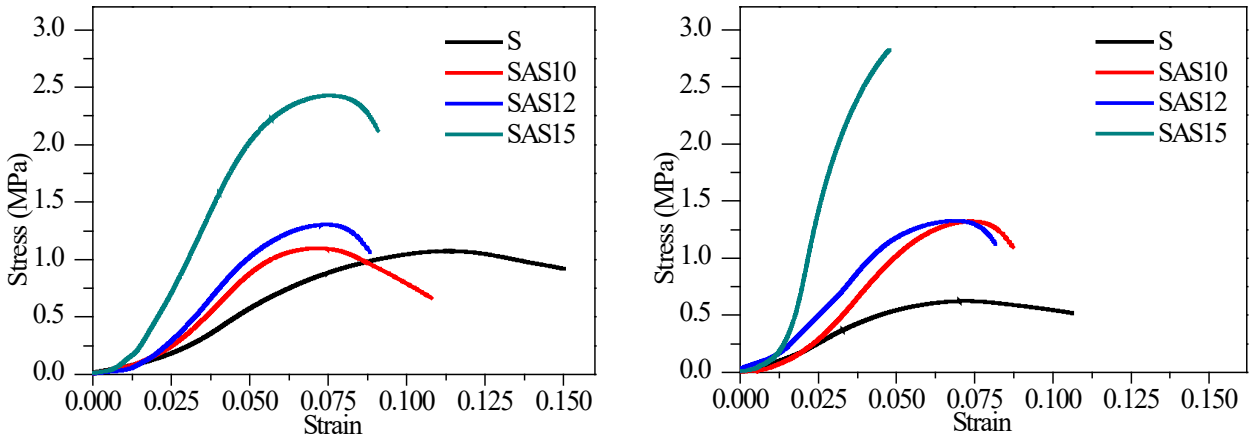

a) Aged 7 d b) Aged 28 d

Figure 3. Stress-strain curves.

variations mentioned above, the continuous hydration of the steel slag leads to the strengthening of the mechanical properties. With an increase in the incorporation of A-SS, the strengthening effect led by the hydration of the steel slag exceeds the weakening effect led by the specific variation, shown overall as the increase in the unconfined compressive strength of the solidified soil.

The strain-stress curves of the solidified soil at 7 d and 28 d are shown in Figure 3. The solidification effects of A-SS lead to an increase in the ultimate failure stress of the solidified soil, which is in accordance with the variations in the unconfined compressive strength. Meanwhile, the ultimate strains of the solidified soil significantly decrease. As shown in Figure 3a, the ultimate strains decrease by 28 %, 41.3 %, and 39.3 % respectively, when 10 %, 12 %, and 15 % A-SS are incorporated at 7 d. When the age reaches 28 d, the effects of the A-SS incorporation on the strains of the solidified soil are similar to that of 7 d. As shown in Figure 3b, the 10 %, 12 % and 15 % A-SS incorporations lead to a decrease in the ultimate strains by 16.9 %, 23.5 % and 54.7 %, respectively. In addition to the changes in the ultimate strains induced by the A-SS incorporation, it should be also noted that the ultimate strain changes with the age. When the age changes from 7 d to 28 d, the ultimate strain of S, SAS10, SAS12, and SAS15 decrease by 29.3 %, 18.5 %, 9.09 %, and 47.3 %, respectively. Although the deformation modulus of the solidified soil is non-linear, it could still be found that the slope of the stress-strain increases with the addition of A-SS, meaning that the incorporation of A-SS leads to an increase in the deformation modules of the saline soil. Based on the stress-strain curves, the fracture energy is calculated and is shown in Table 4. The 10 % and 12 % A-SS incorporation significantly decrease the fracture energy, while the 15 % A-SS incorporation increases the fracture energy at 7 d, whereas, all three A-SS incorporations increase the fracture energy at 28 d.

Table 4. Fracture energy of the specimens (J·m^{-2}).

Age	S	SAS10	SAS12	SAS15
7 d	105.79	71.99	65.54	135.61
28 d	46.22	64.80	67.06	60.70

Ultrasonic test

An ultrasonic test is a well-known non-destructive method for assessing Young's modulus and the internal characteristics of the materials, such as metals, concretes, and wooden materials. It has been confirmed that the response of the ultrasound is in line with the mechanical properties of a stabilised rammed earth wall [20, 22], the ultrasonic test is a valid technique for assessing the quality of stabilised soil.

Figure 4 shows the time required for the ultrasound to pass through the specimens. The incorporations of A-SS show the same effect on the results of the ultrasonic test at different ages, the higher the incorporations of A-SS, the shorter the time required for the ultrasound to pass through the specimens. Based

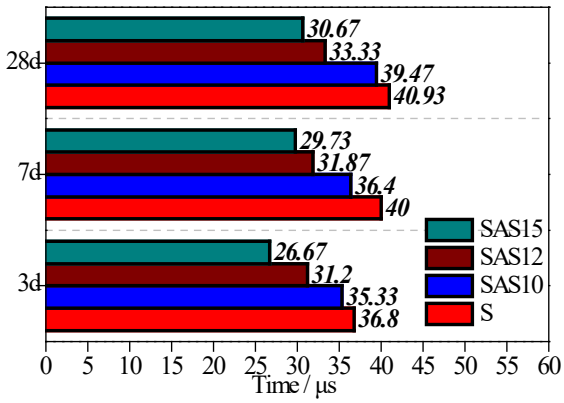

Figure 4. Time required for the ultrasound to pass through the specimens.

on the results shown above, the propagation velocity of the ultrasound in the specimens could be calculated and is reported in Table 5. The stabilised effect of the A-SS significantly increases the propagation velocity of the ultrasound in the solidified soil, especially for SAS15, the degree of the increase reaches 37.8 % at 3 d, 34.5 % at 7 d, and 33.4 % at 28 d, indicating the deformation modulus or the inner porosity are modified by the A-SS incorporation. The former inference is consistent with the finding in Section "Mechanical Properties" where the deformation modulus of the saline soil is effectively increased by the A-SS incorporation, whereas the effect of the A-SS incorporation on the inner porosity needs to be investigated further.

In addition, the propagation velocity of the ultrasound in the specimens decreases with an increase in the age for all the specimens. The propagation velocity of S reduces by 8 % and 10.1 % when the age increases from 3 d to 7 d and 28 d, for SAS15, the propagation velocity reduces by 10.3 % and 13.1 %, respectively. As shown in Figure 2, the deformation modulus of S, SAS10, and SAS12 show no obvious changes with an increase in the age, so it could be speculated that the inner porosities of the specimens increase with age. For SAS15, the deformation modulus increases with the age, thus its inner porosity increases to a greater extent than the others. All the specimens in the study were rammed in the same mode, which guarantees the same compactness for the all samples at the initial age. Thus, the difference in the inner porosity for the samples with the different dosages of the A-SS incorporation and the samples of different ages result from the physical and chemical changes. The microstructures and the compositions of the specimens should be of the main concern.

Table 5. Propagation velocity of the ultrasound ($m \cdot s^{-1}$).

Age	S	SAS10	SAS12	SAS15
3 d	1087	1132	1282	1500
7 d	1000	1099	1255	1345
28 d	977	1013	1200	1304

Morphology of the microstructures

As shown in Figure 5, the microstructures of the specimens with the different A-SS incorporations are quite different at 28 d. The microstructure of S is much looser compared to the others, the soil particles are

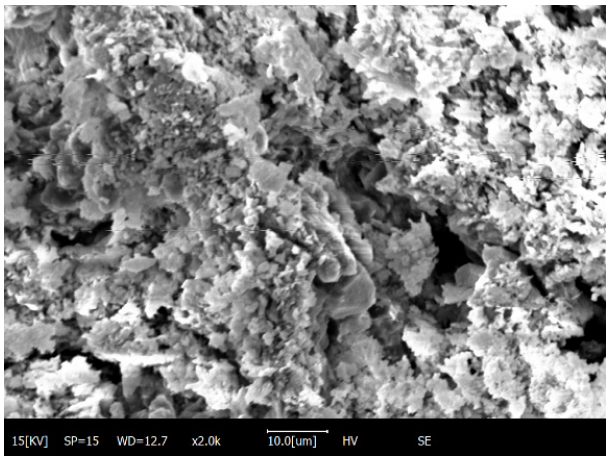

a) S

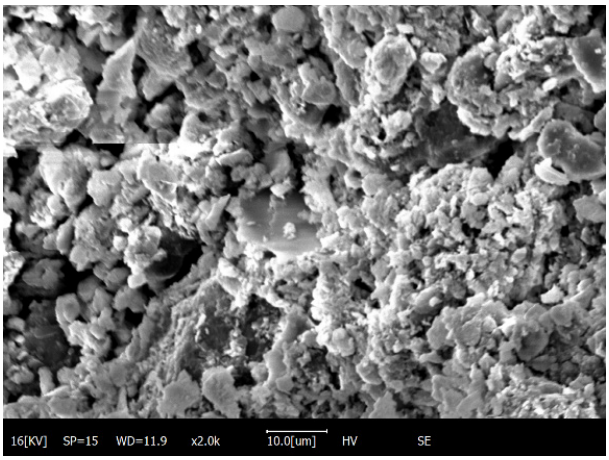

b) SAS10

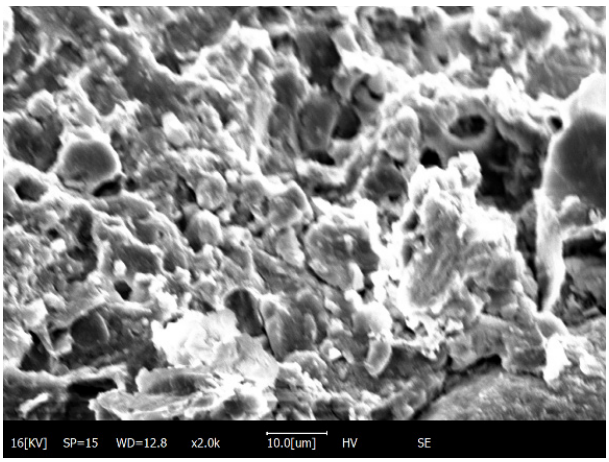

c) SAS12

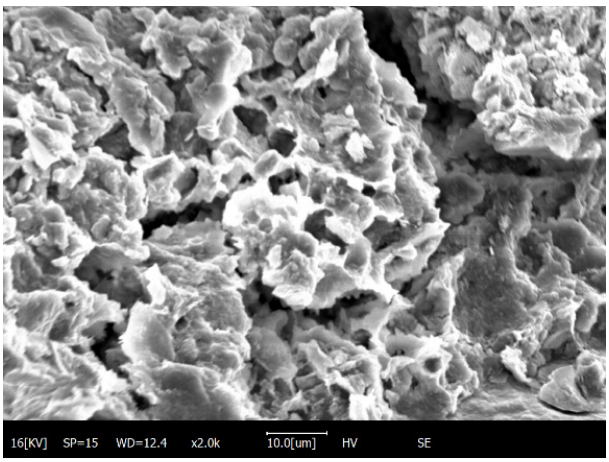

d) SAS15

Figure 5. Morphology of the microstructures at 28 d.

dispersive, few connections exist between the particles. For SAS10, there are some crystals existing among the particles, besides, gelatinous products are also found around some particles. For SAS12 and SAS15, a considerable amount of gelatinous products form on the surfaces of the particles. Dispersive particles can hardly be found in the pictures, the crystals and particles are combined by the formed gelatinous products. Compared to S, the microstructures of SAS12 and SAS15 are denser, and the porosities of the matrix are lower.

The difference in the microstructures of the solidified soil can be interpreted by the increase in the unconfined compressive strength of the solidified soil. The interaction between the soil particles, which is closely related to the macro mechanical properties of soil, mainly comes from the physical adsorption. The stronger the physical adsorption, the higher the mechanical properties. It is well accepted that the specific area of common gelatinous products is far greater than the soil particles. The formation and existence of gelatinous products strengthen the interactions between the particles and, therefore, increase the unconfined compressive strength of the specimens.

XRD Analysis

The XRD patterns of the solidified soil at 7 d and 28 d are shown in Figure 6. Compared to S, the intensity of the C-A-S-H and C-A-H peaks in the solidified soil are stronger, indicating that the incorporations of A-SS significantly promote the formation of C-A-S-H and C-A-H. The mineral phases of the steel slag include C3S, C2S, calcium aluminate, wustite, and amorphous phases, though the phases (C3S, C2S, and calcium aluminate,) are the same as that of cement, the steel slag has poor hydration activity due to the low content of those phases [23, 24]. Under the alkali activation and the hydration of the above reactive phases, some inert Si-O bonds are opened and, therefore, become reactive. Al exists in the calcium aluminate and calcium aluminate silicate phases, with the progress of hydration, the calcium aluminate hydrates and forms C-A-H, it has been verified by the presence of the C-A-S-H gel in the conversion of Si-O-Si to Si-O-Al [19]. Thus, it could be stated that the gelatinous products observed in the microstructure of the solidified soil are C-A-H and C-A-S-H, which cohere the soil particles and strengthen the mechanical properties.

When the age reaches 28 d, the peak intensity of $CaSO_4 \cdot 2H_2O$ and $CaSO_4$ for all the specimens are significantly increased. It could be attributed to the reprecipitation of the relevant ions. As introduced in Section "Raw materials", the optimum moisture content of the saline soil is 20.3 %, whereas its actual moisture content is 10.1 %, additional water was incorporated to make up the difference during the sample preparation process. Part of the $CaSO_4 \cdot 2H_2O$ existing in saline soil dissolves into the water, so the diffraction peaks are weak at 7 d. With an increase in the curing age, the steel slag incorporated into the soil hydrated gradually, and some free water in the soil is sucked and consumed by the hydration of the steel slag or by other reactions, leading to a decrease in the content of the free water, accompanied with an increase in the content of Ca^{2+} and SO_4^{2-} in the solution. When the saturation of the solution, with respect to $CaSO_4 \cdot 2H_2O$, reaches a certain point, the $CaSO_4 \cdot 2H_2O$ would reprecipitate, shown as the higher diffraction peaks in Figure 6b. The growth of the crystals would separate the compact soil particles tamped during the process of the sample preparation and, therefore, leads to a decrease in unconfined compressive and a reduction in the ultrasonic propagation velocity. It could be inferred that the recrystallisation of $CaSO_4 \cdot 2H_2O$ is the specific variation mentioned in Section " Mechanical Properties". Similar to that at 7 d, the peak intensity of C-A-S-H and C-A-H for SAS10, SAS12, and SAS15 are still higher than that of S, meaning that the C-A-S-H and C-A-H formed in the solidified soil are more than the reference, which was verified by the SEM analysis shown in Section "XRD Analysis".

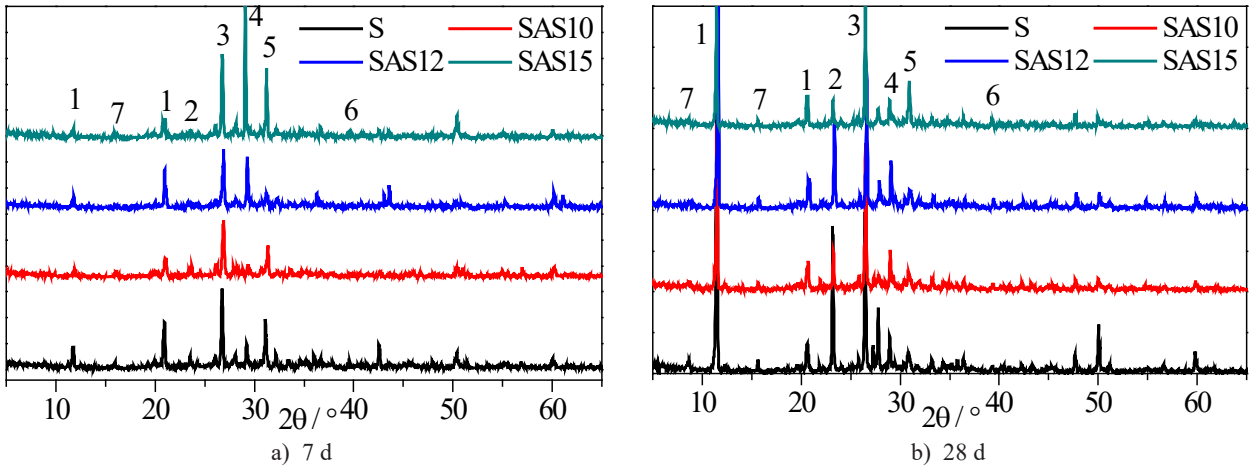

a) 7 d b) 28 d

Figure 6. XRD patterns. (1: $CaSO_4 \cdot 2H_2O$, 2: $CaSO_4$, 3: SiO_2, 4: C-A-S-H, 5: C-A-H, 6: $Al(OH)_3$ 7: Ettringite.)

CONCLUSION

Unconfined compressive strength tests of the saline soil solidified with A-SS and ultrasonic tests were conducted in the study. In addition, the microstructure and chemical compositions of the solidified soil were also investigated. Based on the above results, the conclusions are drawn as follows:

The A-SS incorporation can improve the mechanical properties of the saline soil, especially when the dosage of A-SS incorporation exceeds 15 %, and the unconfined compressive strength of the soil can be significantly increased. The ultrasound propagates faster in the solidified soil than in the original soil.

The microstructure of the solidified soil with the A-SS incorporation is much more compact than the original soil. The soil particles are combined by the formed gelatinous products, C-A-S-H and C-A-H, existing in a continuous form, which accounts for the prominent increase in the unconfined compressive strength and the faster propagation velocity of the ultrasound in the solidified soil.

The solidification of saline soil by alkali-activated steel slag is feasible, but the dosage of the alkali-activated steel slag and the mode of the activation need to be reasonably controlled.

Acknowledgment

The authors would like to acknowledge the financial support of the Qinghai Provincial Science and Technology Department Basic Research Project (2022-ZJ-980Q), and the Qinghai Provincial Key Laboratory of Plateau Green Building and Eco-community Open Fund Project (KLKF-2021-002).

REFERENCES

1. Lv Q. F., Jiang L. S., Ma B., Zhao B. H., Huo Z. S. (2018): A study on the effect of the salt content on the solidification of sulfate saline soil solidified with an alkali-activated geopolymer. *Construction and Building Materials, 204*, 158–165. doi: 10.1016/j.conbuildmat.2018.05.013
2. Zhou Y. X., Yan P. Y. (2007): Investigation on dry shrinkage and wet expansion of solidified saline soil containing different salts. *Chinese Journal of Geotechnical Engineering, 29*(11), 1653–1658 (in Chinese). doi: 10.3321/j.issn:1000-4548.2007.11.010
3. Zhou Y. X., Yan P. Y. (2007): Autogenous volumetric stability of solidified saline soil. *Journal of Tsinghua University (Science and Technology,. 17*(2), 2089-2094 (in Chinese). doi: 10.3321/j.issn:1000-0054.2007.12.002
4. Zhou Y. X., Yan P. Y. (2007): Soil reinforcement techniques and their evolvement. *Journal of Railway Science and Engineering, 3*(4), 35-40 (in Chinese). doi: 10.3969/j.issn.1672-7029.2006.04.007
5. Ying Z., Cui Y. J., Benahmed N., Duc M. (2021): Investigating the salinity effect on water retention property and microstructure changes along water retention curves for lime-treated soil. *Construction and Building Materials, 303*, 124564. doi: 10.1016/j.conbuildmat.2021.124564
6. Houston S. L., Houston W. N., Zapata C. E., Lawrence C. (2001): Geotechnical engineering practice for collapsible soils. *Geotechnical and Geological Engineering, 19*, 333-355. doi: 10.1023/A:1013178226615
7. Deng Y., Yue X., Liu S., Chen Y., Zhang D. (2015): Hydraulic conductivity of cement stabilized marine clay with metakaolin and its correlation with pore size distribution. *Engineering. Geology, 193,* 146–152. doi:10.1016/j.enggeo.2015.04.018
8. Sargent P., Hughes P. N., Rouainia M. (2016): A new low carbon cementitious binder for stabilising weak ground conditions through deep soil mixing. *Soils and Foundations. 56*(6), 1021–1034. doi: 10.1016/j.sandf.2016.11.007
9. Moghadam M. J., Ajalloeian R., Hajiannia A. (2019): Preparation and application of alkali activated materials based on waste glass and coal gangue: A review. *Construction and Building Materials, 221*, 84–98. doi: 10.1016/j.conbuildmat.2019.06.071
10. Zhou H. Y., Wang X. H., Wu Y. P., Zhang X. Y. (2021): Mechanical properties and micro-mechanisms of marine soft soil stabilized by different calcium content precursors based geopolymers. *Construction and Building Materials, 305*, 124722. doi: 10.1016/j.conbuildmat.2021.124722
11. Pourakbar S., Asadi A., Huat B. B. K., Fasihnikoutablab M. H. (2014) : Stabilization of clayey soil using ultrafine palm oil fuel ash (POFA) and cement. *Transportation Geotechnics, 3*, 24–35. doi: 10.1016/j.trgeo.2015.01.002
12. Al-Amoudi O. S. B. (2002): Characterization and chemical stabilization of Al-Qurayyah Sabkha soil. *Journal of Materials in Civil Engineering, 14*(6), 478–484. doi: 10.1061/(ASCE)0899-1561(2002)14:6(478)
13. Chai S. X., Wang X. Y., Wei L., Wang P. (2009): Appreciation of strength and suitability of five solidified saline soils in inshore. *Journal of Liaoning Technical University, 28*, 59-62 (in Chinese). doi: 10.3969/j.issn.1008-0562.2009.01.017
14. Jamsawang P., Poorahong H., Yoobanpot N., Songpiriyakij S., Jongpradist P. (2017). Improvement of soft clay with cement and bagasse ash waste. *Construction and Building Materials, 154*, 61–71. doi: 10.1016/j.conbuildmat.2017.07.188
15. Horpibulsuk S., Phetchuay C., Chinkulkijniwat A. (2012). Soil stabilization by calcium carbide residue and fly ash. *Journal of Materials in Civil Engineering, 24*, 184–193. doi: 10.1061/(ASCE)MT.1943-5533.0000370
16. Zhang Y. J., Liu C. L., Xu Y., Wang Y. C., Xu D. L. (2012): A new alkali–activated steel slag–based cementitious material for photocatalytic degradation of organic pollutant from waste water. *Journal of Hazardous Materials, 209–210*, 146–150. doi: 10.1016/j.jhazmat.2012.01.001
17. Zhang Y.J., He P.Y., Chen H. (2018): A novel CdO/graphene alkali–activated steel slag nanocomposite for photocatalytic degradation of dye wastewater. *Ferroelectrics, 522*(1), 1–8. doi: 10.1080/00150193.2017.1391587
18. Wang Q., Yang J.W., Yan P. Y. (2012): Influence of initial alkalinity on the hydration of steel slag. *Science China: Technological Sciences, 55*(12), 3378–3387. doi: 10.1007/s11431-012-4830-9

19. Liu Z., Zhang D., Li L., et al. (2019): Microstructure and phase evolution of alkali–activated steel slag during early age. *Construction and Building Materials, 204*, 158–165. doi: 10.1016/j.conbuildmat.2019.01.213
20. Han F. H., Zhang Z. Q. (2018): Properties of 5-year-old concrete containing steel slag powder. *Powder Technology, 334*, 27-35. doi: 10.1016/j.powtec.2018.04.054
21. Canivell J., Martìn-del-Rio J., Alejandre F. J., Garcìa-Heras J., Jimenez-Aguilar A. (2018): Considerations on the physical and mechanical properties of lime-stabilized rammed earth walls and their evaluation by ultrasonic pulse velocity testing. *Construction and Building Materials, 191*, 826–836. doi: 10.1016/j.conbuildmat.2018.09.207
22. Martìn-del-Rio J., Canivell J., Falcón R. M. (2020): The use of non-destructive testing to evaluate the compressive strength of a lime-stabilised rammed-earth wall: Rebound index and ultrasonic pulse velocity. *Construction and Building Materials, 242*, 118060. doi: 10.1016/j.conbuildmat.2020.118060
23. Zhuang S. Y., Wang Q. (2021): Inhibition mechanisms of steel slag on the early-age hydration of cement. *Cement and Concrete Research, 140*, 106283. doi: 10.1016/j.cemconres.2020.106283
24. Sun J. W., Zhang Z. Q. Zhuang S. Y., He W. (2020): Hydration properties and microstructure characteristics of alkali-activated steel slag. *Construction and Building Materials, 241*, 118141. doi: 10.1016/j.conbuildmat.2020.118141